
PERGAMON

Journal of the Mechanics and Physics of Solids
50 (2002) 2463–2493

JOURNAL OF THE
MECHANICS AND
PHYSICS OF SOLIDS

www.elsevier.com/locate/jmps

Stability of thermally-induced martensitic transformations in bi-atomic crystals

Ryan S. Elliott, John A. Shaw, Nicolas Triantafyllidis *

Department of Aerospace Engineering, University of Michigan, Ann Arbor, MI 48109, USA

Received 24 July 2001; received in revised form 29 January 2002; accepted 12 February 2002

Abstract

Some of the most interesting, and technologically important solid–solid transformations are the first order diffusionless transformations that occur in certain equiatomic, ordered, bi-atomic crystals. These displacive transformations include thermally-induced, reversible, proper martensitic transformations as seen in shape memory alloys such as NiTi (where group–subgroup relationships exist between the symmetry groups of the crystal phases) and the reconstructive martensitic transformations seen in certain ionic compounds such as CsCl (where no group–subgroup relationship exists between the phases).

In contrast to existing continuum mechanics approaches, the present work constructs a continuum energy density function $W(\mathbf{F},\theta)$ (as a function of a uniform deformation gradient and temperature) of a perfect periodic bi-atomic crystal from temperature-dependent atomic pair-potentials. Equilibrium solutions and their stability are examined as a function of temperature for crystals under no external stress. The full problem is solved numerically, and an asymptotic theory is employed to guide the numerical solution near multiple bifurcation points. Using pair-potentials and enforcing constrained kinematics (uniform deformation of a cubic CsCl-type crystal), lower symmetry crystals, such as orthorhombic, monoclinic, and rhombohedral structures are predicted. The first two of these are unstable within the chosen temperature window for our particular case, while the third is stable for higher temperatures. In addition, a hysteretic transformation was discovered in which the CsCl structure is stable at high temperatures and the NaCl structure is stable at low temperatures. These two cubic phases are connected by an unstable rhombohedral path corresponding to the transformation mechanism proposed by Buerger (1951). The CsCl–NaCl transformation suggested by the numerical results is a reconstructive transformation with a group–nonsubgroup relationship between the symmetry groups of the two phases. © 2002 Elsevier Science Ltd. All rights reserved.

Keywords: A. Phase transformation; A. Thermomechanical processes; B. Finite strain; C. Stability and bifurcation; C. Asymptotic analysis

* Corresponding author. Tel.: +1-734-763-2356; fax: +1-734-763-0578.
E-mail address: nick@engin.umich.edu (N. Triantafyllidis).

0022-5096/02/$ - see front matter © 2002 Elsevier Science Ltd. All rights reserved.
PII: S0022-5096(02)00012-1

1. Introduction

Although there is no universal agreement on classification (for example, contrast Cohen et al. (1979), Tolédano and Dmitriev (1996), James (1986)), solid–solid phase transformations can be (loosely) divided into two categories diffusional and diffusionless, depending on whether long-range atomic migration is involved. Adopting the classification scheme of Cohen et al. (1979), diffusionless transformations (also called displacive transformations) can be subdivided into two major categories, shuffle transformations which involve no macroscopic strain, and lattice-distortive transformations, which involve a macroscopic strain of the lattice. If a (relatively) undistorted interface plane exists between the phases for lattice-distortive transformations, the transformation is called martensitic.

We choose to further classify martensitic transitions as either "*proper*" martensitic transformations, where a group–subgroup relationship exists between the symmetry groups of the parent and product phases (a requirement for shape memory behavior, see Bhattacharya, 1998), or as "*reconstructive*" martensitic transitions, where no such group–subgroup relationship exists (see Tolédano and Dmitriev, 1996). In the proper martensitic case the austenite (high symmetry) and martensite (low symmetry) crystals are connected kinematically by infinitesimal displacements of atoms (these transformations are often reversible). Reconstructive martensitic transitions on the other hand involve finite displacements and often the breaking and reforming of atomic bonds. Reversible proper martensitic transformations are seen in shape memory alloys (SMAs) such as NiTi and have been the subject of intensive study in recent years due to their potential for novel technological applications. Reconstructive martensitic transformations are seen in steel, in many pure elements (BCC–HCP and BCC–FCC transitions), in several compounds such as CsCl and other alkali-halides (CsCl–NaCl), and AgI and CuBr (both BCC-wurtzite).

This work was originally motivated by an interest in thermoelastic proper martensitic transformations seen in NiTi. However as will be seen, the approach taken applies equally well to the reconstructive type of martensitic transformation. Many of the characteristics of such transformations imply difficulties for theoretical models at the continuum length-scale. For instance, the tendency in SMAs for the transition from the austenite phase to the martensite phase to occur through the mechanism of localization and propagation of transformation fronts, shows that instabilities at the nano-scale can percolate all the way up to the macro-scale, even for polycrystalline SMAs (Shaw and Kyriakides, 1998; Shaw, 2000). The modeling of discontinuous strain fields implies serious technical problems, since the governing equilibrium equations are no longer elliptic in nature.

A continuum mechanics framework of finite strain thermoelasticity has emerged since the 1980s, thanks to the work of Abeyaratne, Bhattacharya, Ericksen, James, Knowles and many others. It consists of postulating a phenomenological energy density $W(\mathbf{F};\theta)$ (where $\mathbf{F}$ is the deformation gradient tensor and θ is the absolute temperature of the material at the point of interest), whose local minima with respect to $\mathbf{F}$ (potential wells) correspond to different phases of the crystal. For the general three-dimensional formulation of the corresponding boundary value problems and the appropriate requirements

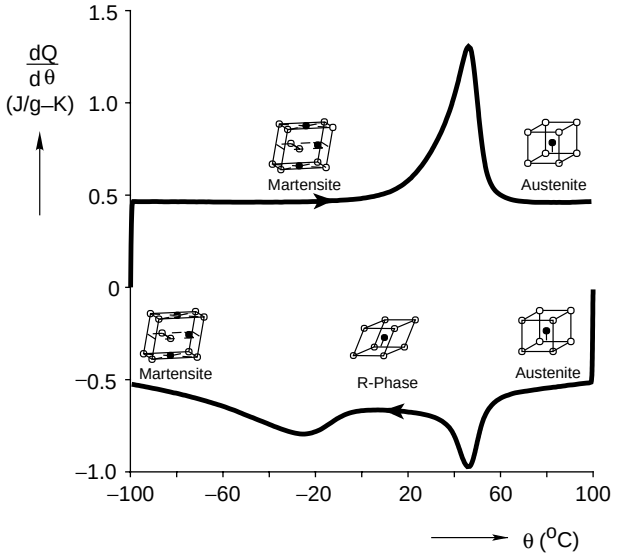

Fig. 1. Differential scanning calorimetry of NiTi wire, showing solid state phases with different crystal symmetries; austenite (B2 or CsCl cubic), R-phase (rhombohedral), martensite (B19′ or monoclinic).

for $W(\mathbf{F};\theta)$, the interested reader is referred to James (1986). The main objective of these investigations is to give the general form of W for these crystals and to study the nature of the solutions for corresponding boundary value problems. This approach has successfully predicted many features of the fine microstructures observed experimentally in shape memory crystals (e.g., the laminar microstructures in CuAlNi investigated by Abeyaratne et al., 1996). The same continuum mechanics framework has also been considered by Ericksen (1992), who used symmetry properties of the crystals to show the possibility of bifurcated equilibrium paths.

Unfortunately, the phenomenological construction of W leaves some important questions unanswered pertaining to which phases can coexist at a certain temperature. The continuum mechanics literature thus far deals with constructions where two distinct phases (and all their variants) are assumed: a highly symmetric austenite crystal, usually cubic, and a lower symmetry martensite crystal, such as tetragonal, rhombohedral, orthorhombic, or monoclinic. For some shape memory materials of interest, such as NiTi with particular heat treatment, three different stable phases (and all their variants) can coexist, i.e. cubic, monoclinic, and rhombohedral (see the differential scanning calorimetry thermogram of Fig. 1). The phenomenological constructions of such energy densities, although feasible become exceedingly complex and unmanageable. Additional related questions, which cannot be answered by the above phenomenological models without supplementary assumptions, pertain to the relative size (compared to the lattice) of the wavelength of twinning modes at the nano-scale and interfacial energies at boundaries between phases.

For our purposes we return to the underlying nano-structure and derive the corresponding energy density from temperature-dependent atomic potentials. We prefer to avoid the usual approach of molecular dynamics with its statistical aspects and large-scale computations, and instead model phenomena in a quasi-static setting. This also allows us to find all equilibrium paths and address their stability in a systematic way. First order gradient (local) continuum calculations for nonlinear periodic crystals are frequently encountered in the physics and materials science literature, in particular when elastic properties of crystals based on atomistic pair-potentials are sought. The earliest studies of stability of mono-atomic cubic crystals under finite strains go back to Born (1940). Somewhat more recently, in a series of articles Milstein (1970) and Milstein and Hill (1977, 1978, 1979) used the same approach to study the dependence of bulk and shear moduli on pressure and examined the stability of these crystals. To the best of the authors' knowledge, no systematic effort has been devoted to modeling martensitic transformations by explicitly deriving an energy density function $W(\mathbf{F};\theta)$ from a network of temperature-dependent atomic potentials and to study the ensuing symmetry-breaking bifurcated equilibrium solutions and their stability.

The goal of the present work is to use atomistic model simulations as a tool for generating an energy density $W(\mathbf{F};\theta)$ of a prototype, ordered, bi-atomic, crystal (CsCl structure). Such an energy density has all the necessary symmetry properties of the underlying crystal and is used to find all the equilibrium phases and their stability within a certain temperature range. Accordingly, Section 2 introduces our atomic model and the scope of the boundary value problem of interest. Section 3 details the stability analysis and asymptotic solutions near critical points in the equilibrium paths. Section 4 provides numerical results for a particular bi-atomic crystals maps all the equilibrium paths for crystals of different symmetries, and determines their stability.

2. Formulation

2.1. Problem statement

Since the focus of the current work is to determine the bulk behavior of a perfect, equi-atomic, ordered crystal of two elements, we restrict our attention to the behavior of an infinite crystal under uniform deformation. We chose the CsCl (or B2) structure as our reference configuration. The relative position vector $\mathbf{r}_{ij}$, separating atom i and atom j, is given by $\mathbf{r}_{ij}=\mathbf{F}\cdot[\mathbf{X}_j-\mathbf{X}_i]$ where $\mathbf{X}_i$ is the reference position of atom i. The symbol $(\cdot)$ indicates tensor contraction, where $\mathbf{F}\cdot\mathbf{X}$ represents $F_{ik}X_k$ in component form with Einstein's summation convention. The rigid body rotation part, $\mathbf{R}$, of the deformation gradient tensor $\mathbf{F}=\mathbf{R}\cdot\mathbf{U}$ is irrelevant for a uniform deformation, so without loss of generality it is assumed to be $\mathbf{R}=\mathbf{I}$, the rank two identity tensor. Consequently,

$$\mathbf{r}_{ij}=\mathbf{U}\cdot[\mathbf{X}_j-\mathbf{X}_i], \tag{2.1}$$

where $\mathbf{U}$ is the uniform, symmetric right stretch tensor. It is recognized that martensitic transformations in SMAs, for example, involve internal atomic shuffles (e.g., the B19′

structure of NiTi martensite shown in Fig. 1, see also Otsuka et al., 1971), but these locally nonuniform deformations, as well as twinning deformation are left to future work. The energy density of the crystal, therefore, is given by the summation of the atomic potential of atom i, ϕ_i, over a reference volume of the unit cell, V_r, as

$$W(\mathbf{U};\theta) = \frac{1}{2V_r}\sum_{i=1}^{K}\phi_i(\mathbf{r}_{i1},\mathbf{r}_{i2},\ldots,\mathbf{r}_{i(i-1)},\mathbf{r}_{i(i+1)},\ldots;\theta), \tag{2.2}$$

where K is the number of atoms per unit cell and the arguments of ϕ_i reflect the possible interactions with all other atoms.

We are presently interested in temperature-induced transformations under no externally applied stress. Temperature, in this case, plays the role of the only loading parameter. Equilibrium solutions are sought of a stress-free, perfect crystal (specifically, the CsCl structure as seen in NiTi austenite) and its stability in a 100 K, or so, interval about the reference temperature of 300 K. Equilibrium paths are found by extremizing W with respect to the right stretch tensor $\mathbf{U}$, or

$$\frac{\partial W}{\partial \mathbf{U}} = \mathbf{0}. \tag{2.3}$$

The fundamental hypothesis is that martensitic transformations are manifestations of lattice level instabilities in certain crystals. For example, the remarkable behavior of SMAs is a result of material existing at the cusp of an instability that causes a sort of "buckling" of the crystal structure. For a conservative system in equilibrium stability is evaluated in the usual way by determining whether $\partial^2 W/\partial\mathbf{U}\partial\mathbf{U}$ is positive definite along the equilibrium paths found from Eq. (2.3), or

$$\min\left[\delta\mathbf{U}:\frac{\partial^2 W}{\partial\mathbf{U}\partial\mathbf{U}}:\delta\mathbf{U}\right] > 0, \tag{2.4}$$

for all admissible, second-order, symmetric tensors $\delta\mathbf{U}$, and where $\mathbf{A}$:$\mathbf{B}$ denotes double tensor right contraction (defined in component form as $A_{ijkl}B_{kl}$).

2.2. Atomistic model

The simplest way to model atomic interactions is by the pair-potential model. We recognize the well known deficiencies inherent in the use of pair-potentials (Cauchy relations, etc.) but accept these limitations in the interest of simplicity. Thus, the atomic potential of atom i can be written as the sum of pair-potentials for all the interacting atoms.

$$\phi_i(\mathbf{r}_{i1},\mathbf{r}_{i2},\ldots;\theta) = \phi_i(r_{i1};\theta) + \phi_i(r_{i2};\theta) + \cdots, \tag{2.5}$$

where r_{ij} is the length of $\mathbf{r}_{ij}$.

The energy of an ordered equi-atomic CsCl crystal (with atom species a and b) is thus constructed by summing over the interacting atom pairs within a sphere of

influence.

$$W(\mathbf{U};\theta) = \frac{1}{2V_r}\left[\sum_i (\phi_{aa}(r_{ai};\theta) + \phi_{ab}(r_{bi};\theta)) + \sum_j (\phi_{bb}(r_{bj};\theta) + \phi_{ab}(r_{aj};\theta))\right], \quad (2.6)$$

where ϕ_{aa}, ϕ_{ab}, and ϕ_{bb} denote the pair-potentials between atoms a–a, a–b, and b–b, respectively and the subscripts a and b on r denote the corresponding atoms in a unit cell. Here i and j range over all a and b atoms, respectively. A sphere of influence is chosen to represent the distance outside of which interactions are considered negligible. In this way the model includes long-range central-force interactions at the nano-scale. Any of the popular atomic potentials could be used in this framework, but we selected the following Morse potential, [1]

$$\phi(r) = A\left\{\exp\left[-2m\left(\frac{r}{r_0} - 1\right)\right] - 2\exp\left[-m\left(\frac{r}{r_0} - 1\right)\right]\right\}, \quad (2.7)$$

where r is the current separation between two atoms, r_0 is the zero force separation, and A and m are parameters characterizing the strength and stiffness of the bond. The Morse potential is chosen for convenience, since it rapidly (exponentially) decays with radius. The bond is made temperature-dependent by assuming the parameters to be temperature-dependent as follows:

$$\phi(r;\theta) = A(\theta)\left\{\exp\left[-2m(\theta)\left(\frac{r}{\hat{r}(\theta)} - 1\right)\right] - 2\exp\left[-m(\theta)\left(\frac{r}{\hat{r}(\theta)} - 1\right)\right]\right\}, \quad (2.8)$$

where

$$A(\theta) = A_0\left[1 - \frac{\theta}{4\theta_m}\right], \qquad m(\theta) = m_0\left[1 + \alpha_\theta\frac{(\theta - \theta_r)}{\theta_r}\right], \qquad \hat{r}(\theta) = r_0\left[1 - \frac{1}{2m_0}\ln\left(1 - \frac{\theta}{4\theta_m}\right)\right],$$

θ_r—reference temperature,
r_0—bond length at $\theta = 0$,
θ_m—melting temperature,
A_0—binding energy,
m_0—bond stiffness parameter,
α_θ—stiffness temperature coefficient. (2.9)

[1] It is understood that interaction potentials and their coefficients depend on bond type a–a, a–b, and b–b, but these indices are omitted to avoid cumbersome notation in Eqs. (2.7)–(2.9).

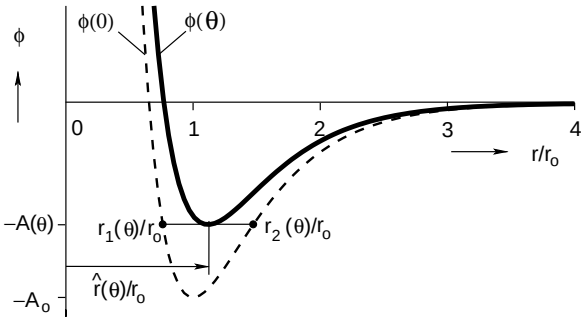

Fig. 2. Temperature-dependent bonds.

This specific form of ϕ arises from the construction shown in Fig. 2. An absolute zero temperature bond potential has the parameters A_0, m_0, and r_0. As thermal energy (kinetic energy according to $nk\theta$, where k is Boltzmann's constant and n is the number of degrees of freedom of the bond) is added the energy of the bond increases linearly with temperature above the zero temperature binding energy of $-A_0$. The Morse potential has an inflection point (zero bond stiffness) at the energy of $-3A_0/4$, so the thermal energy $A_0/4$ is interpreted as the approximate energy required for melting. In order to avoid the necessity of dynamic simulations, we choose an average natural bond length according to $\hat{r}(\theta) = [r_1(\theta) + r_2(\theta)]/2$, where r_1 and r_2 are the extreme bond lengths under thermal oscillations at θ. A Morse-type, temperature-dependent, quasi-static atomic potential is constructed to have a minimum at this average position and is scaled to have the total energy of the bond. With increasing temperature this effectively results in a slight increase in the natural bond length (due to the asymmetry of the bond potential). In addition, the bond stiffness parameter m is assumed to have a linear dependence with temperature (according to the parameter α_θ) in the neighborhood of a chosen reference temperature θ_r. Specific parameters for the three bond types will be discussed in the numerical results presented in Section 4.

3. Asymptotic analysis

Eq. (2.3) may appear disarmingly simple, but it actually represents six nonlinear equilibrium equations. The case when the stability criterion Eq. (2.4) is equal to zero defines a critical point on the equilibrium path. As will be seen certain critical points may have multiple bifurcation modes, and the treatment of such a complication is an important feature of the present work. In order to guide our numerical solution of Eq. (2.3) and to provide an analytical verification of our numerical results, an asymptotic analysis of the bifurcated paths near critical points is required. The approach taken here is based on the Lyapunov–Schmidt–Koiter decomposition and follows the general

theory given in Triantafyllidis and Peek (1992), which is used to find critical points, categorize their type, and find the initial stability of emanating branches. [2]

3.1. Critical points

The stress-free equilibrium states sought are the solutions of Eq. (2.3). Due to the cubic symmetry of the crystal, an obvious solution is the CsCl crystal structure with a uniform dilation, $\overset{0}{\mathbf{U}}(\theta) = \lambda(\theta)\mathbf{I}$. We refer to this as the "*principal solution*". The principal solution, $\overset{0}{\mathbf{U}}(\theta)$, is assumed to be stable for high temperatures, at least in a neighborhood of the reference temperature, θ_r. Accordingly, it is a local minimizer of the energy, W, and hence $\partial^2 W/\partial\mathbf{U}\partial\mathbf{U}$ evaluated on $\overset{0}{\mathbf{U}}(\theta)$ is positive definite.

As the temperature decreases away from θ_r, it reaches a value θ_c, called the "*critical temperature*", at which the austenitic phase, $\overset{0}{\mathbf{U}}(\theta)$, is no longer a local energy minimizer and the positive definiteness of $\partial^2 W/\partial\mathbf{U}\partial\mathbf{U}$ along the principal solution is lost, i.e.,

$$\overset{2}{\mathbf{L}}{}^{c} : \overset{(I)}{\mathbf{U}} = \mathbf{0}; \quad (I = 1, \ldots, N), \tag{3.1}$$

where

$$\overset{2}{\mathbf{L}}{}^{c} \equiv \frac{\partial^2 W(\overset{0}{\mathbf{U}}(\theta_c); \theta_c)}{\partial\mathbf{U}\partial\mathbf{U}}, \tag{3.2}$$

represents the tangent moduli tensor at the critical point, and N is the order of the critical point. [3] The N eigenmodes, [4] $\overset{(I)}{\mathbf{U}}$, are a basis for the null space of $\overset{2}{\mathbf{L}}{}^{c}$. From here on capital Latin indices $(I,J,K,\ldots)$ refer to eigenmodes, whereas lower Latin indices $(i,j,k,\ldots)$ refer to Cartesian directions.

3.2. Cubic symmetry

While an explicit knowledge of the elastic energy density, $W(\mathbf{F};\theta)$, is assumed, much can be learned about the character of critical points based solely on the material symmetry properties of W. The cubic symmetry of the reference configuration implies that the energy density must satisfy

$$W(\mathbf{F};\theta) = W(\mathbf{F}\cdot\mathbf{M};\theta), \tag{3.3}$$

---

[2] The interested reader is also referred to Ericksen (1996), which presents an equivalent analysis for the tetragonal mono-atomic lattice under applied pressure and temperature, but from a somewhat different viewpoint.

[3] From here on a superscript or subscript "c" indicates that the quantity is evaluated at the critical temperature, θ_c.

[4] In view of the major symmetry of $\overset{2}{\mathbf{L}}{}^{c}$, there are N linearly independent eigenmodes, where N is the multiplicity of the corresponding zero eigenvalue of $\overset{2}{\mathbf{L}}{}^{c}$.

where, $\mathbf{M} \in \mathcal{O}$, the octahedral point symmetry group, which consists of all rigid body transformations mapping a cube onto itself. The deformation gradient, $\mathbf{F}$, may be written $\mathbf{R} \cdot \mathbf{U}$ by virtue of the polar decomposition theorem, where $\mathbf{R}$ is a rigid body rotation and $\mathbf{U}$, the right stretch tensor, is symmetric. Since we make use of the uniform deformation assumption, $\mathbf{R}$ may be chosen arbitrarily, and thus, the energy density may be considered a function of $\mathbf{U}$ only. Furthermore, the principle of frame indifference states that $W(\mathbf{F};\theta) = W(\mathbf{R} \cdot \mathbf{F};\theta)$ for any rotation $\mathbf{R}$. Now, since $\mathbf{M}$ is a rigid body transformation, so is its transpose (inverse), $\mathbf{M}^{\mathrm{T}}$, and we may take $\mathbf{R} = \mathbf{M}^{\mathrm{T}}$ resulting in a symmetric argument $\mathbf{M}^{\mathrm{T}} \cdot \mathbf{U} \cdot \mathbf{M}$. The cubic symmetry requirements on the energy density can now be restated with symmetric tensor arguments as

$$W(\mathbf{U};\theta) = W(\mathbf{M}^{\mathrm{T}} \cdot \mathbf{U} \cdot \mathbf{M};\theta) \tag{3.4}$$

for all $\mathbf{M} \in \mathcal{O}$. The energy density is then invariant under an arbitrary permutation of the indices of the components of $\mathbf{U}$ and a sign change of two of the three shear components of $\mathbf{U}$. That is (no sums are implied),

$$\begin{aligned} W(\mathbf{U};\theta) &= W(U_{ii}, U_{jj}, U_{kk}, U_{ij}, U_{jk}, U_{ki};\theta) \\ &= W(U_{ii}, U_{jj}, U_{kk}, -U_{ij}, -U_{jk}, U_{ki};\theta) \\ &= W(U_{ii}, U_{jj}, U_{kk}, -U_{ij}, U_{jk}, -U_{ki};\theta) \\ &= W(U_{ii}, U_{jj}, U_{kk}, U_{ij}, -U_{jk}, -U_{ki};\theta), \end{aligned} \tag{3.5}$$

where $\{i,j,k\}$ is any permutation of $\{1,2,3\}$. Thus, Eq. (3.5) represents 24 relations that can be used to simplify the asymptotic expansions used below.

Any pure dilation, $\overset{0}{\mathbf{U}}(\theta) = \lambda(\theta)\mathbf{I}$, leaves the cubic symmetry of the crystal unchanged. A Taylor series expansion of the energy density[5] can be constructed about the pure dilation $\overset{0}{\mathbf{U}}(\theta)$, and a lengthy calculation results in

$$\begin{aligned} W(\overset{0}{\mathbf{U}}(\theta) + \Delta\mathbf{U};\theta) = {} & \overset{0}{L} + \overset{1}{L}_n \sum_i \Delta U_{ii} \\ & + \frac{1}{2!}\left(\overset{2}{L}_{nn} \sum_i (\Delta U_{ii})^2 + \overset{2}{L}_{nn'} \sum_{i \neq j} (\Delta U_{ii} \Delta U_{jj}) + \overset{2}{L}_{ss} \sum_{i \neq j} 2(\Delta U_{ij})^2 \right) \\ & + \frac{1}{3!}\left(\overset{3}{L}_{nnn} \sum_i (\Delta U_{ii})^3 + \overset{3}{L}_{nnn'} \sum_{i \neq j} 3((\Delta U_{ii})^2 \, \Delta U_{jj}) \right. \end{aligned}$$

[5] It is assumed that W is sufficiently smooth.

$$+\overset{3}{L}_{nn'n''}\sum_{i\neq j\neq k\neq i}(\Delta U_{ii}\Delta U_{jj}\Delta U_{kk})+\overset{3}{L}_{nss}\sum_{i\neq j}12(\Delta U_{ii}(\Delta U_{ij})^2)$$

$$+\overset{3}{L}_{n'ss}\sum_{i\neq j\neq k\neq i}6(\Delta U_{ii}(\Delta U_{jk})^2)+\overset{3}{L}_{ss's''}\sum_{i\neq j\neq k\neq i}8(\Delta U_{ij}\Delta U_{ik}\Delta U_{jk})\Bigg)$$

$$+O(\boldsymbol{\Delta}\mathbf{U}^4). \tag{3.6}$$

The notation used in Eq. (3.6) requires some explanation. We define $\overset{K}{\mathbf{L}}$ as the $2K$th order tensor, representing the Kth partial derivative of the energy density with respect to the right stretch tensor evaluated on the principal branch, i.e.,

$$\overset{K}{\mathbf{L}}(\overset{0}{\mathbf{U}}(\theta);\theta)\equiv\frac{\partial^K W(\overset{0}{\mathbf{U}}(\theta);\theta)}{\partial\mathbf{U}^K}. \tag{3.7}$$

A subscript "n" represents a *normal* component of the stretch tensor with a pair of equal indices (11, or 22, or 33), such as $\overset{2}{L}_{nn}=\partial^2 W/\partial U_{11}\partial U_{11}$. A subscript "$s$" represents a *shear* component of the stretch tensor with a pair of unequal indices (12, 23, 31, 21, 32, 13), such as $\overset{2}{L}_{ss}=\partial^2 W/\partial U_{12}\partial U_{12}$. In some cases it is necessary to use subscripts with a prime ($'$) to indicate that a pair of indices are distinct from those indices which do not have a prime, for example $\overset{2}{L}_{nn'}=\partial^2 W/\partial U_{11}\partial U_{22}$. Three mutually distinct pairs of indices are indicated with a prime and a double prime ($''$). See Table 1 for a list of the symbols used in Eq. (3.6), giving an example of each.

3.3. Classification of critical points

To determine the character (bifurcation or limit load) of the critical points which may be encountered, use of the notation introduced in Eq. (3.6) leads to the restatement of the critical point definition in Eq. (3.1) as follows:

$$\begin{bmatrix}\overset{2}{L}{}^c_{nn} & \overset{2}{L}{}^c_{nn'} & \overset{2}{L}{}^c_{nn'} & 0 & 0 & 0\\ \overset{2}{L}{}^c_{nn'} & \overset{2}{L}{}^c_{nn} & \overset{2}{L}{}^c_{nn'} & 0 & 0 & 0\\ \overset{2}{L}{}^c_{nn'} & \overset{2}{L}{}^c_{nn'} & \overset{2}{L}{}^c_{nn} & 0 & 0 & 0\\ 0 & 0 & 0 & \overset{2}{L}{}^c_{ss} & 0 & 0\\ 0 & 0 & 0 & 0 & \overset{2}{L}{}^c_{ss} & 0\\ 0 & 0 & 0 & 0 & 0 & \overset{2}{L}{}^c_{ss}\end{bmatrix}\begin{bmatrix}U_{11}\\ U_{22}\\ U_{33}\\ 2U_{12}\\ 2U_{23}\\ 2U_{31}\end{bmatrix}^{(I)}=\mathbf{0};\quad (I=1,\ldots,N). \tag{3.8}$$

Table 1
Nonzero components in expansion (3.6)

Tensor	Order	Example	Nonzero equal components
$\overset{1}{\mathbf{L}}$	2nd	$\overset{1}{L}_n = \dfrac{\partial W}{\partial U_{11}}$	3
$\overset{2}{\mathbf{L}}$	4th	$\overset{2}{L}_{nn} = \dfrac{\partial^2 W}{\partial U_{11}\partial U_{11}}$	3
		$\overset{2}{L}_{nn'} = \dfrac{\partial^2 W}{\partial U_{11}\partial U_{22}}$	6
		$\overset{2}{L}_{ss} = \dfrac{\partial^2 W}{\partial U_{12}\partial U_{12}}$	12
$\overset{3}{\mathbf{L}}$	6th	$\overset{3}{L}_{nnn} = \dfrac{\partial^3 W}{\partial U_{11}\partial U_{11}\partial U_{11}}$	3
		$\overset{3}{L}_{nnn'} = \dfrac{\partial^3 W}{\partial U_{11}\partial U_{11}\partial U_{22}}$	18
		$\overset{3}{L}_{nn'n''} = \dfrac{\partial^3 W}{\partial U_{11}\partial U_{22}\partial U_{33}}$	6
		$\overset{3}{L}_{nss} = \dfrac{\partial^3 W}{\partial U_{11}\partial U_{12}\partial U_{12}}$	72
		$\overset{3}{L}_{n'ss} = \dfrac{\partial^3 W}{\partial U_{11}\partial U_{23}\partial U_{23}}$	36
		$\overset{3}{L}_{ss's''} = \dfrac{\partial^3 W}{\partial U_{11}\partial U_{23}\partial U_{31}}$	48

Nontrivial solutions exist when the determinant of the coefficient matrix is zero,

$$(\overset{2}{L}{}^c{}_{nn} + 2\overset{2}{L}{}^c{}_{nn'})(\overset{2}{L}{}^c{}_{nn} - \overset{2}{L}{}^c{}_{nn'})^2(\overset{2}{L}{}^c{}_{ss})^3 = 0. \tag{3.9}$$

There are three[6] distinct cases of order $N = 1$, 2, and 3, respectively, according to the multiplicity of the root of Eq. (3.9). For each case, the character of the critical point is determined by the following criterion (see Triantafyllidis and Peek, 1992),

$$\left.\frac{\partial^2 W}{\partial \mathbf{U}\partial\theta}\right|_c \overset{(I)}{:}\mathbf{U} \begin{cases} \neq 0, \text{ limit load point,} \\ =0, \text{ bifurcation point,} \end{cases} \tag{3.10}$$

which tests whether or not the equilibrium path passing through the critical point is unique. Each of the three possible solutions of Eq. (3.9) is now classified in turn.

[6] Simultaneous roots, such as $\overset{2}{L}{}^c{}_{nn} - \overset{2}{L}{}^c{}_{nn'} = \overset{2}{L}{}^c{}_{ss} = 0$ are not investigated due to their degenerate and unlikely nature.

Case I. $\overset{2}{L}{}^{c}_{nn} + 2\overset{2}{L}{}^{c}_{nn'} = 0.$

In this case the critical point is of order $N = 1$ with a single eigenmode, $\overset{(1)}{\mathbf{U}} = \mathbf{I}$, a simple dilation. According to Eqs. (3.6) and (3.10),

$$\left.\frac{\partial^2 W}{\partial \mathbf{U}\partial\theta}\right|_c : \overset{(1)}{\mathbf{U}} = \left.\frac{\partial \overset{1}{L}{}_n}{\partial\theta}\right|_c \operatorname{tr} \overset{(1)}{\mathbf{U}} = 3 \left.\frac{\partial L^1{}_n}{\partial\theta}\right|_c \neq 0, \tag{3.11}$$

a critical point of this type is a *limit load.*

Case II. $\overset{2}{L}{}^{c}_{nn} = \overset{2}{L}{}^{c}_{nn'}.$

In this case, where the two normal moduli are equal, the critical point is of order $N = 2$ with two independent eigenmodes,

$$\overset{(1)}{\mathbf{U}} = \begin{bmatrix} 2 & 0 & 0 \\ 0 & -1 & 0 \\ 0 & 0 & -1 \end{bmatrix}, \quad \overset{(2)}{\mathbf{U}} = \begin{bmatrix} -1 & 0 & 0 \\ 0 & 2 & 0 \\ 0 & 0 & -1 \end{bmatrix}. \tag{3.12}$$

Examination of criterion (3.10) shows

$$\left.\frac{\partial^2 W}{\partial \mathbf{U}\partial\theta}\right|_c : \overset{(I)}{\mathbf{U}} = \left.\frac{\partial \overset{1}{L}{}_n}{\partial\theta}\right|_c \operatorname{tr} \overset{(I)}{\mathbf{U}} = 0, \quad (I = 1, 2). \tag{3.13}$$

This case, therefore, corresponds to a *double bifurcation point*.

Case III. $\overset{2}{L}{}^{c}_{ss} = 0.$

In this case, where the shear modulus vanishes, the critical point is of order $N = 3$ with three independent eigenmodes,

$$\overset{(1)}{\mathbf{U}} = \begin{bmatrix} 0 & 0 & 0 \\ 0 & 0 & 1 \\ 0 & 1 & 0 \end{bmatrix}, \quad \overset{(2)}{\mathbf{U}} = \begin{bmatrix} 0 & 0 & 1 \\ 0 & 0 & 0 \\ 1 & 0 & 0 \end{bmatrix}, \quad \overset{(3)}{\mathbf{U}} = \begin{bmatrix} 0 & 1 & 0 \\ 1 & 0 & 0 \\ 0 & 0 & 0 \end{bmatrix}. \tag{3.14}$$

Criterion (3.10) in this case shows

$$\left.\frac{\partial^2 W}{\partial \mathbf{U}\partial\theta}\right|_c : \overset{(I)}{\mathbf{U}} = \left.\frac{\partial \overset{1}{L}{}_n}{\partial\theta}\right|_c \operatorname{tr} \overset{(I)}{\mathbf{U}} = 0, \quad (I = 1, 2, 3), \tag{3.15}$$

which indicates that the critical point is a *triple bifurcation point*.

3.4. Bifurcated branches and their initial stability

The initial stability of the bifurcated branches associated with Case II and Case III is now examined using the asymptotic analysis of Triantafyllidis and Peek (1992). According to the general theory, any bifurcated equilibrium path can be expressed in

terms of a *bifurcation amplitude*, ξ. The deformation measure $\mathbf{U}$ and temperature θ for each equilibrium path are parameterized in terms of ξ. The corresponding asymptotic expansions near the critical point $(\overset{0}{\mathbf{U}}(\theta_c), \theta_c)$ are

$$\mathbf{U}(\xi) = \overset{0}{\mathbf{U}}(\theta(\xi)) + \xi \overset{1}{\mathbf{U}}_c + \frac{\xi^2}{2} \overset{2}{\mathbf{U}}_c + O(\xi^3), \tag{3.16a}$$

$$\theta(\xi) = \theta_c + \xi\theta_1 + \frac{\xi^2}{2}\theta_2 + O(\xi^3). \tag{3.16b}$$

In the case where $\theta_1 \neq 0$ (called a *transcritical*, or *asymmetric*, bifurcation) only the linear terms are required to determine the equilibrium paths and their stability near θ_c, where

$$\overset{1}{\mathbf{U}}_c = \sum_{I=1}^{N} \alpha_I \overset{(I)}{\mathbf{U}}, \tag{3.17a}$$

$$\|\boldsymbol{\alpha}\| = 1, \tag{3.17b}$$

and $\boldsymbol{\alpha}$ (not to be confused with the scalar lattice angle, α) is the unit tangent of the bifurcated equilibrium path at the critical point with dimensionality equal to the order of the bifurcation point. There are as many unit tangents, $\boldsymbol{\alpha}$, as bifurcated equilibrium paths through θ_c. However, if $\theta_1 = 0$ identically (called a *super-critical* or *sub-critical*, or *symmetric*, bifurcation) the second order terms are needed. In this case,

$$\overset{2}{\mathbf{U}}_c = \sum_{I,J=1}^{N} \alpha_I \alpha_J \overset{(IJ)}{\mathbf{V}}, \tag{3.18}$$

where $\overset{(IJ)}{\mathbf{V}}$ is defined by

$$\left.\frac{\partial^2 W}{\partial \mathbf{U} \partial \mathbf{U}}\right|_c : \overset{(IJ)}{\mathbf{V}} = -\left(\left.\frac{\partial^3 W}{\partial \mathbf{U} \partial \mathbf{U} \partial \mathbf{U}}\right|_c : \overset{(I)}{\mathbf{U}}\right) : \overset{(J)}{\mathbf{U}}, \tag{3.19a}$$

$$\overset{(IJ)}{\mathbf{V}} : \overset{(K)}{\mathbf{U}} = 0. \tag{3.19b}$$

The first condition, (3.19a), is necessary to satisfy equilibrium involving order ξ^2 terms, and the last condition, (3.19b), ensures the uniqueness of $\overset{(IJ)}{\mathbf{V}}$ by choosing it to be orthogonal to $\overset{(K)}{\mathbf{U}}$. Combining the equilibrium equations in the null space of $\overset{2}{\mathbf{L}}^c$ with the above asymptotic expressions for the displacement $\mathbf{U}$ (3.16)–(3.18) results in the following system of equilibrium equations for the $\boldsymbol{\alpha}$'s.

$$\text{If } \theta_1 \neq 0\text{:} \quad \sum_{J,K=1}^{N} \alpha_J \alpha_K \mathscr{E}_{IJK} + 2\theta_1 \sum_{J=1}^{N} \alpha_J \mathscr{E}_{IJ\theta} = 0; \quad (I = 1, \ldots, N), \tag{3.20a}$$

$$\text{If } \theta_1 = 0\text{:} \quad \sum_{J,K,L=1}^{N} \alpha_J \alpha_K \alpha_L \mathscr{E}_{IJKL} + 3\theta_2 \sum_{J=1}^{N} \alpha_J \mathscr{E}_{IJ\theta} = 0; \quad (I = 1,\ldots,N). \tag{3.20b}$$

The coefficients $\mathscr{E}_{IJK}$, $\mathscr{E}_{IJKL}$, and $\mathscr{E}_{IJ\theta}$ are defined as $(I,J,K,L = 1,\ldots,N)$,

$$\mathscr{E}_{IJK} \equiv \left[\frac{\partial^3 W}{\partial U_{ij}\partial U_{kl}\partial U_{mn}}\right]_c \overset{(I)}{U}_{ij} \overset{(J)}{U}_{kl} \overset{(K)}{U}_{mn}, \tag{3.21a}$$

$$\mathscr{E}_{IJKL} \equiv \left[\frac{\partial^4 W}{\partial U_{ij}\partial U_{kl}\partial U_{mn}\partial U_{pq}}\right]_c \overset{(I)}{U}_{ij} \overset{(J)}{U}_{kl} \overset{(K)}{U}_{mn} \overset{(L)}{U}_{pq} + \left[\frac{\partial^3 W}{\partial U_{ij}\partial U_{kl}\partial U_{mn}}\right]_c \left(\overset{(J)}{U}_{kl} \overset{(KL)}{V}_{mn} + \overset{(K)}{U}_{kl} \overset{(JL)}{V}_{mn} + \overset{(L)}{U}_{kl} \overset{(JK)}{V}_{mn} \right) \overset{(I)}{U}_{ij}, \tag{3.21b}$$

$$\mathscr{E}_{IJ\theta} \equiv \left[\frac{\mathrm{d}}{\mathrm{d}\theta}\left(\frac{\partial^2 W(\overset{0}{\mathbf{U}}(\theta);\theta)}{\partial U_{ij}\partial U_{kl}}\right)\right]_c \overset{(I)}{U}_{ij} \overset{(J)}{U}_{kl}. \tag{3.21c}$$

The initial stability of bifurcated equilibrium paths is governed, according to the general theory, by the properties of the matrix **B**, defined as

$$\text{If } \theta_1 \neq 0\text{:} \quad B_{IJ}(\boldsymbol{\alpha}) \equiv \theta_1 \mathscr{E}_{IJ\theta} + \sum_{K=1}^{N} \alpha_K \mathscr{E}_{IJK}, \tag{3.22a}$$

$$\text{If } \theta_1 = 0\text{:} \quad B_{IJ}(\boldsymbol{\alpha}) \equiv \theta_2 \mathscr{E}_{IJ\theta} + \sum_{K,L=1}^{N} \alpha_K \alpha_L \mathscr{E}_{IJKL}. \tag{3.22b}$$

The initial stability of a symmetric ($\theta_1 = 0$) bifurcated equilibrium branch is guaranteed if **B** is positive definite. Asymmetric ($\theta_1 \neq 0$) bifurcated equilibrium branches have a change in stability as the critical point is crossed if all eigenvalues of **B** are of the same sign, but they are initially unstable in both directions if the signs of the eigenvalues are different. We now revisit the two different types of bifurcation paths found in Section 3.3, determine their tangents $\boldsymbol{\alpha}$, and examine their initial stability.

Case II. $\overset{2}{L}{}^c_{nn} = \overset{2}{L}{}^c_{nn'}$, $N = 2$.

This case is a double bifurcation point, which has at most three[7] bifurcated paths intersecting the primary branch at θ_c. From the corresponding eigenmodes in Eq. (3.12) and the expansion of the energy density (3.6) one finds for $\mathscr{E}_{IJK}$ and $\mathscr{E}_{IJ\theta}$, according to the definitions (3.21a) and (3.21c)

$$\mathscr{E}_{IJK} = \begin{cases} \mathscr{E}, & I = J = K, \\ -\mathscr{E}/2, & \text{otherwise}, \end{cases} \tag{3.23a}$$

[7] Since Eq. (3.20a) is a system of N quadratic equations for $\boldsymbol{\alpha}$, there are as many as $2^N - 1$ nontrivial independent real solutions (the trivial solution is, of course, the principal branch).

$$\mathscr{E}_{IJ\theta} = \begin{cases} \mathscr{E}_\theta, & I = J, \\ -\mathscr{E}_\theta/2, & \text{otherwise}, \end{cases} \tag{3.23b}$$

where

$$\mathscr{E} \equiv 6(\overset{3}{L}{}^{c}_{nnn} - 3\overset{3}{L}{}^{c}_{nnn'} + 2\overset{3}{L}{}^{c}_{nn'n''}), \tag{3.24a}$$

$$\mathscr{E}_\theta \equiv 6\,\frac{\mathrm{d}}{\mathrm{d}\theta}(\overset{2}{L}_{nn} - \overset{2}{L}_{nn'})_c. \tag{3.24b}$$

It should be noted that the derivative in Eq. (3.24b) is a total derivative with respect to θ (see definition (3.7)).

With the help of the above result, the system of equations (3.20a) which governs the initial tangent, $\boldsymbol{\alpha}$, of each bifurcated equilibrium path can be simplified to

$$\theta_1\mathscr{E}_\theta(2\alpha_1 - \alpha_2) + \mathscr{E}(\alpha_1^2 - \alpha_1\alpha_2 - \alpha_2^2/2) = 0, \tag{3.25a}$$

$$\theta_1\mathscr{E}_\theta(2\alpha_2 - \alpha_1) + \mathscr{E}(\alpha_2^2 - \alpha_1\alpha_2 - \alpha_1^2/2) = 0. \tag{3.25b}$$

By inspection, the above system has 3 real solutions: $\mathscr{T}_1, \mathscr{T}_2, \mathscr{T}_3$, representing asymmetric (tetragonal, as will be seen) equilibrium paths, all with the same nonzero θ_1,

$$\mathscr{T}_1\text{:}\quad \boldsymbol{\alpha} = (1,0), \qquad \theta_1 = -\mathscr{E}/2\mathscr{E}_\theta, \tag{3.26a}$$

$$\mathscr{T}_2\text{:}\quad \boldsymbol{\alpha} = (0,1), \qquad \theta_1 = -\mathscr{E}/2\mathscr{E}_\theta, \tag{3.26b}$$

$$\mathscr{T}_3\text{:}\quad \boldsymbol{\alpha} = (-1,-1), \quad \theta_1 = -\mathscr{E}/2\mathscr{E}_\theta, \tag{3.26c}$$

where the convenient norm $\|\boldsymbol{\alpha}\|_\infty$ was chosen. According to the eigenmodes (3.12) and the linear term in the asymptotic expansion (3.16a), the bifurcated branches emerge from the principal branch with tangents

$$\overset{1}{\mathbf{U}}_c(\mathscr{T}_1) = \begin{bmatrix} 2 & 0 & 0 \\ 0 & -1 & 0 \\ 0 & 0 & -1 \end{bmatrix}, \quad \overset{1}{\mathbf{U}}_c(\mathscr{T}_2) = \begin{bmatrix} -1 & 0 & 0 \\ 0 & 2 & 0 \\ 0 & 0 & -1 \end{bmatrix}, \quad \overset{1}{\mathbf{U}}_c(\mathscr{T}_3) = \begin{bmatrix} -1 & 0 & 0 \\ 0 & -1 & 0 \\ 0 & 0 & 2 \end{bmatrix}. \tag{3.27}$$

The above equilibrium paths are the three variants of a tetragonal phase (sides $a=b\neq c$, angles $\alpha=\beta=\gamma=\pi/2$) which results by stretching a cubic cell of the austenitic phase along one axis.

The stability of these asymmetric paths in the neighborhood of θ_c is found using the 2×2 matrix $\mathbf{B}$ defined by Eq. (3.22a). Using the results of Eq. (3.23) we obtain for

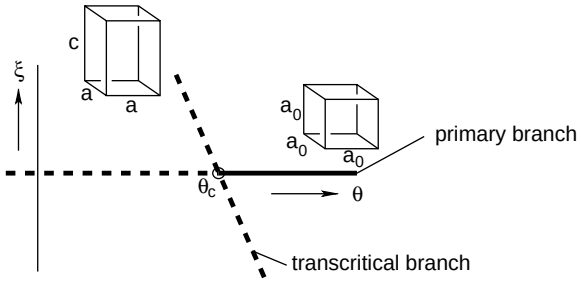

Fig. 3. Cubic to tetragonal bifurcation.

the three paths,

$$\mathbf{B}(\mathscr{T}_1)=\frac{\mathscr{E}}{4}\begin{bmatrix}2 & -1\\ -1 & -4\end{bmatrix},\quad \mathbf{B}(\mathscr{T}_2)=\frac{\mathscr{E}}{4}\begin{bmatrix}-4 & -1\\ -1 & 2\end{bmatrix},\quad \mathbf{B}(\mathscr{T}_3)=\frac{\mathscr{E}}{4}\begin{bmatrix}-4 & 5\\ 5 & -4\end{bmatrix}. \tag{3.28}$$

Since the determinant of each one of the above matrices is strictly negative, the corresponding two eigenvalues are of different sign and hence all the corresponding transverse bifurcation paths from cubic to tetragonal are unstable in the neighborhood of θ_c. This is a rather strong result, since it depends only on the cubic symmetry of the primary branch and not on the particular form of the chosen energy density. A schematic of this type of transformation is depicted in Fig. 3.

Case III. $\overset{2}{L}{}^{c}_{ss}=0,\ N=3.$

This case is a triple bifurcation point with at most $2^N-1=7$ bifurcated branches emerging from θ_c. From the corresponding eigenmodes (3.14) and the expansion (3.6), we find $\mathscr{E}_{IJK}$ and $\mathscr{E}_{IJ\theta}$ $(I,J,K=1,\ldots,N)$ defined in Eqs. (3.21a), (3.21c) to be

$$\mathscr{E}_{IJK}=\begin{cases}\mathscr{E}, & I\neq J\neq K\neq I,\\ 0, & \text{otherwise},\end{cases} \tag{3.29a}$$

$$\mathscr{E}_{IJ\theta}=\begin{cases}\mathscr{E}_\theta, & I=J,\\ 0, & \text{otherwise},\end{cases} \tag{3.29b}$$

where

$$\mathscr{E}\equiv 8\,\overset{3}{\mathbf{L}}{}^{c}_{ss's''}, \tag{3.30a}$$

$$\mathscr{E}_\theta\equiv 4\,\frac{\mathrm{d}}{\mathrm{d}\theta}\left(\overset{2}{L}_{ss}\right)_c. \tag{3.30b}$$

With the help of the above result, the equilibrium equations (3.20a) simplify to

$$\theta_1 \mathscr{E}_\theta \alpha_1 + \mathscr{E} \alpha_2 \alpha_3 = 0, \tag{3.31a}$$

$$\theta_1 \mathscr{E}_\theta \alpha_2 + \mathscr{E} \alpha_3 \alpha_1 = 0, \tag{3.31b}$$

$$\theta_1 \mathscr{E}_\theta \alpha_3 + \mathscr{E} \alpha_1 \alpha_2 = 0. \tag{3.31c}$$

By inspection, we find that the above system has 7 real solutions, divided into two categories, according to whether $\alpha_1\alpha_2\alpha_3 \neq 0$ (4 rhombohedral solutions $\mathscr{RH}_1, \ldots, \mathscr{RH}_4$) or $\alpha_1\alpha_2\alpha_3 = 0$ (3 orthorhombic solutions $\mathscr{OR}_1, \mathscr{OR}_2, \mathscr{OR}_3$). The equilibrium paths in the first category are the asymmetric bifurcated branches, all with the same nonzero θ_1 satisfying

$$\mathscr{RH}_1\text{:} \quad \boldsymbol{\alpha} = (-1,-1,-1)/\sqrt{3}, \quad \theta_1 = \mathscr{E}/\sqrt{3}\mathscr{E}_\theta, \tag{3.32a}$$

$$\mathscr{RH}_2\text{:} \quad \boldsymbol{\alpha} = (-1,1,1)/\sqrt{3}, \quad \theta_1 = \mathscr{E}/\sqrt{3}\mathscr{E}_\theta, \tag{3.32b}$$

$$\mathscr{RH}_3\text{:} \quad \boldsymbol{\alpha} = (1,-1,1)/\sqrt{3}, \quad \theta_1 = \mathscr{E}/\sqrt{3}\mathscr{E}_\theta, \tag{3.32c}$$

$$\mathscr{RH}_4\text{:} \quad \boldsymbol{\alpha} = (1,1,-1)/\sqrt{3}, \quad \theta_1 = \mathscr{E}/\sqrt{3}\mathscr{E}_\theta, \tag{3.32d}$$

where the convenient norm $\|\boldsymbol{\alpha}\|_2$ was chosen. According to the eigenmodes (3.14) and the linear term in the asymptotic expansion (3.16a), the bifurcated branches emerge from the principal branch with tangents

$$\overset{1}{\mathbf{U}}_c(\mathscr{RH}_1) = \frac{1}{\sqrt{3}}\begin{bmatrix} 0 & -1 & -1 \\ -1 & 0 & -1 \\ -1 & -1 & 0 \end{bmatrix}, \quad \overset{1}{\mathbf{U}}_c(\mathscr{RH}_2) = \frac{1}{\sqrt{3}}\begin{bmatrix} 0 & 1 & 1 \\ 1 & 0 & -1 \\ 1 & -1 & 0 \end{bmatrix},$$

$$\overset{1}{\mathbf{U}}_c(\mathscr{RH}_3) = \frac{1}{\sqrt{3}}\begin{bmatrix} 0 & 1 & -1 \\ 1 & 0 & 1 \\ -1 & 1 & 0 \end{bmatrix}, \quad \overset{1}{\mathbf{U}}_c(\mathscr{RH}_4) = \frac{1}{\sqrt{3}}\begin{bmatrix} 0 & -1 & 1 \\ -1 & 0 & 1 \\ 1 & 1 & 0 \end{bmatrix}. \tag{3.33}$$

The above equilibrium paths are the four variants of a rhombohedral phase (sides $a = b = c$, angles $\alpha = \beta = \gamma$), i.e., stretching the cubic cell along one of its four main diagonals. The stability of these paths in the neighborhood of θ_c is found with the help of the 3×3 matrix $\mathbf{B}$ defined by Eq. (3.22a). Substituting Eqs. (3.29) and (3.32) into Eq. (3.22a) (where now $I,J = 1,2,3$) we obtain

$$\mathbf{B}(\mathscr{RH}_1) = \frac{\mathscr{E}}{\sqrt{3}}\begin{bmatrix} 1 & 1 & 1 \\ 1 & 1 & 1 \\ 1 & 1 & 1 \end{bmatrix}, \quad \mathbf{B}(\mathscr{RH}_2) = \frac{\mathscr{E}}{\sqrt{3}}\begin{bmatrix} 1 & 1 & 1 \\ 1 & 1 & -1 \\ 1 & -1 & 1 \end{bmatrix},$$

$$\mathbf{B}(\mathscr{RH}_3) = \frac{\mathscr{E}}{\sqrt{3}}\begin{bmatrix} 1 & 1 & -1 \\ 1 & 1 & 1 \\ -1 & 1 & 1 \end{bmatrix}, \quad \mathbf{B}(\mathscr{RH}_4) = \frac{\mathscr{E}}{\sqrt{3}}\begin{bmatrix} 1 & -1 & 1 \\ -1 & 1 & 1 \\ 1 & 1 & 1 \end{bmatrix}. \tag{3.34}$$

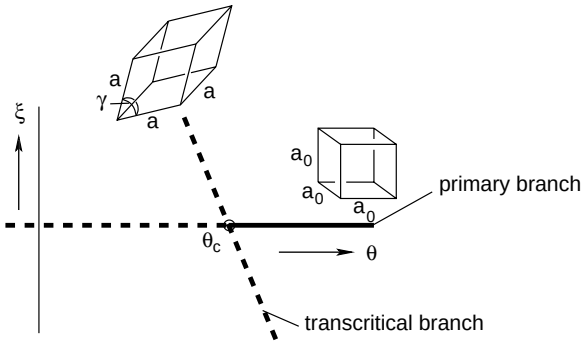

Fig. 4. Cubic to rhombohedral bifurcation.

It is easily checked that each one of the above matrices has two eigenvalues with differing signs, and hence, all the rhombohedral paths are unstable near θ_c. This is again a result independent of the chosen energy density; it only depends on the cubic symmetry of the principal branch. The stability and transverse character of the rhombohedral equilibrium paths are displayed in Fig. 4.

The equilibrium paths through θ_c that belong to the second category of solutions (i.e., $\alpha_1\alpha_2\alpha_3 = 0$) are symmetric branches with

$$\mathcal{OR}_1\text{:} \quad \boldsymbol{\alpha} = (1,0,0), \quad \theta_1 = 0, \tag{3.35a}$$

$$\mathcal{OR}_2\text{:} \quad \boldsymbol{\alpha} = (0,1,0), \quad \theta_1 = 0, \tag{3.35b}$$

$$\mathcal{OR}_3\text{:} \quad \boldsymbol{\alpha} = (0,0,1), \quad \theta_1 = 0. \tag{3.35c}$$

Since $\theta_1 = 0$, Eqs. (3.20b) must be considered to determine the character of these modes. With the help of the expansion (3.6) and eigenmodes (3.14) and the definitions (3.21b) and (3.19) we find

$$\mathscr{E}_{IJKL} = \begin{cases} \hat{\mathscr{E}} & I = J = K = L, \\ \tilde{\mathscr{E}} & I = J \neq K = L \quad \text{or any permutation}, \\ 0 & \text{otherwise}, \end{cases} \tag{3.36}$$

where

$$\hat{\mathscr{E}} \equiv 16\overset{4}{L}{}^{c}_{ssss} + 12(\eta\overset{3}{L}{}^{c}_{n'ss} + 2\hat{\eta}\overset{3}{L}{}^{c}_{nss}), \tag{3.37a}$$

$$\tilde{\mathscr{E}} \equiv 16\overset{4}{L}{}^{c}_{sss's'} + 4((\eta + \hat{\eta})\overset{3}{L}{}^{c}_{nss} + \hat{\eta}\overset{3}{L}{}^{c}_{n'ss}). \tag{3.37b}$$

See Appendix A for details of the calculations of Eqs. (3.37) and the definitions of η and $\hat{\eta}$. After substituting Eq. (3.36), Eqs. (3.20b) simplify to

$$\alpha_1[\hat{\mathscr{E}}\alpha_1^2 + 3\tilde{\mathscr{E}}(\alpha_2^2 + \alpha_3^2) + 3\theta_2\mathscr{E}_\theta] = 0, \tag{3.38a}$$

$$\alpha_2[\hat{\mathscr{E}}\alpha_2^2 + 3\tilde{\mathscr{E}}(\alpha_1^2 + \alpha_3^2) + 3\theta_2\mathscr{E}_\theta] = 0, \tag{3.38b}$$

$$\alpha_3[\hat{\mathscr{E}}\alpha_3^2 + 3\tilde{\mathscr{E}}(\alpha_1^2 + \alpha_2^2) + 3\theta_2\mathscr{E}_\theta] = 0. \tag{3.38c}$$

The above equilibrium system is satisfied by the orthorhombic solutions $\mathscr{O}\mathscr{R}_1, \mathscr{O}\mathscr{R}_2, \mathscr{O}\mathscr{R}_3$ in Eq. (3.35), each case admitting the solution

$$\theta_2 = -\hat{\mathscr{E}}/3\mathscr{E}_\theta. \tag{3.39}$$

Thus, according to the eigenmodes (3.14) and the linear and second order terms in the expansion (3.16a), the bifurcated branches emerge from the principal branch with tangents and curvatures

$$\overset{1}{\mathbf{U}}_c(\mathscr{O}\mathscr{R}_1) = \begin{bmatrix} 0 & 0 & 0 \\ 0 & 0 & 1 \\ 0 & 1 & 0 \end{bmatrix}, \quad \overset{2}{\mathbf{U}}_c(\mathscr{O}\mathscr{R}_1) = \begin{bmatrix} \eta & 0 & 0 \\ 0 & \hat{\eta} & 0 \\ 0 & 0 & \hat{\eta} \end{bmatrix}, \tag{3.40a}$$

$$\overset{1}{\mathbf{U}}_c(\mathscr{O}\mathscr{R}_2) = \begin{bmatrix} 0 & 0 & 1 \\ 0 & 0 & 0 \\ 1 & 0 & 0 \end{bmatrix}, \quad \overset{2}{\mathbf{U}}_c(\mathscr{O}\mathscr{R}_2) = \begin{bmatrix} \hat{\eta} & 0 & 0 \\ 0 & \eta & 0 \\ 0 & 0 & \hat{\eta} \end{bmatrix}, \tag{3.40b}$$

$$\overset{1}{\mathbf{U}}_c(\mathscr{O}\mathscr{R}_3) = \begin{bmatrix} 0 & 1 & 0 \\ 1 & 0 & 0 \\ 0 & 0 & 0 \end{bmatrix}, \quad \overset{2}{\mathbf{U}}_c(\mathscr{O}\mathscr{R}_3) = \begin{bmatrix} \hat{\eta} & 0 & 0 \\ 0 & \hat{\eta} & 0 \\ 0 & 0 & \eta \end{bmatrix}. \tag{3.40c}$$

The above three equilibrium paths correspond to the six variants of an orthorhombic phase (sides $a=b\neq c$, angle $\gamma\neq\pi/2$, $\alpha=\beta=\pi/2$). Each results by shearing two opposite faces of the cube and allowing the perpendicular direction to stretch independently. There are six variants, since each equilibrium path in Eqs. (3.35) corresponds to two variants of the orthorhombic phase (see Fig. 5); one for the angle $\gamma < \pi/2$ and the other for $\gamma > \pi/2$ (i.e., for bifurcation amplitude $\xi < 0$ or $\xi > 0$).

The stability of these paths in the neighborhood of θ_c is found with the help of the 3×3 matrix $\mathbf{B}$ defined by Eq. (3.22b). Substituting Eqs. (3.29), (3.35), and (3.36) into Eq. (3.22b) we obtain,

$$\mathbf{B}(\mathscr{O}\mathscr{R}_1) = \frac{1}{3}\begin{bmatrix} 2\hat{\mathscr{E}} & 0 & 0 \\ 0 & 3\tilde{\mathscr{E}} - \hat{\mathscr{E}} & 0 \\ 0 & 0 & 3\tilde{\mathscr{E}} - \hat{\mathscr{E}} \end{bmatrix}, \quad \mathbf{B}(\mathscr{O}\mathscr{R}_2) = \frac{1}{3}\begin{bmatrix} 3\tilde{\mathscr{E}} - \hat{\mathscr{E}} & 0 & 0 \\ 0 & 2\hat{\mathscr{E}} & 0 \\ 0 & 0 & 3\tilde{\mathscr{E}} - \hat{\mathscr{E}} \end{bmatrix},$$

$$\mathbf{B}(\mathscr{O}\mathscr{R}_3) = \frac{1}{3}\begin{bmatrix} 3\tilde{\mathscr{E}} - \hat{\mathscr{E}} & 0 & 0 \\ 0 & 3\tilde{\mathscr{E}} - \hat{\mathscr{E}} & 0 \\ 0 & 0 & 2\hat{\mathscr{E}} \end{bmatrix}. \tag{3.41}$$

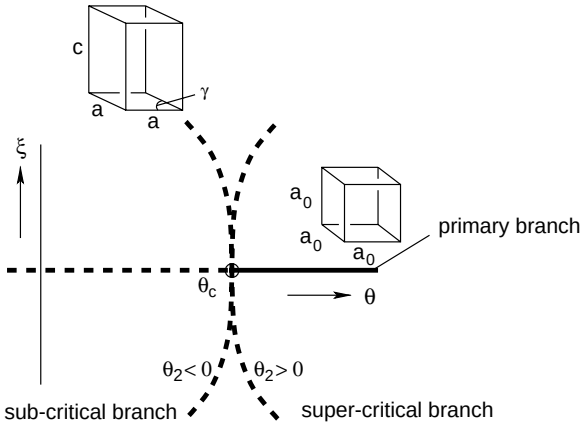

Fig. 5. Cubic to orthorhombic bifurcation.

Positive definiteness of $\mathbf{B}(\boldsymbol{\alpha})$ along a path with initial tangent $\boldsymbol{\alpha}$ guarantees the stability of that path near θ_c. Thus, stability of the orthorhombic paths is guaranteed only when $3\tilde{\mathscr{E}} > \hat{\mathscr{E}} > 0$. Notice that unlike the tetragonal or rhombohedral paths, which were always unstable near θ_c (independent of the particular functional dependence of W), the stability of the orthorhombic paths depends on the choice of atomic interaction potential.

4. Numerical results

Now that a clear understanding exists of the character of equilibrium paths in the vicinity of critical points we turn to numerical calculations of entire equilibrium paths. Table 2 lists the chosen parameters for the pair-potentials introduced in Section 2.2. The *a–a* and *b–b* interactions (like bonds) are chosen to give reasonable elastic moduli and thermal expansion coefficients of pure intermetallics (we chose Ni and Ti) near room temperature. The parameters for the pair-potential of the *a–b* (unlike) bond are then chosen so that the crystal is stable in the CsCl crystal structure at and above the reference temperature of 300 K. The radius associated with the isolated unlike-pair bond is assumed to be the average of the other two bond radii, i.e., $\hat{r}_{ab}(\theta)=[\hat{r}_{aa}(\theta)+\hat{r}_{bb}(\theta)]/2$. The exponents in the like bonds are chosen to be temperature independent ($\alpha_\theta = 0$), yet the exponent of the unlike bond is chosen to decrease linearly with decreasing temperature ($\alpha_\theta > 0$). A pictorial representation of these potentials for the three different type bonds at two different temperatures is given in Fig. 6.

4.1. Solution procedure

As indicated previously the crystal lattice is assumed to follow a uniform deformation $\mathbf{U}$, which is described by six independent components in general. Equivalently, the

Table 2
Pair-potential parameters used in numerical calculation

Parameter	*a–a* bond	*b–b* bond	*a–b* bond
r_0	1	1.16	1.08
θ_m	1718	1943	1573
A_0	1	1.124	0.425
m_0	4	7	5.5
α_θ	0	0	3

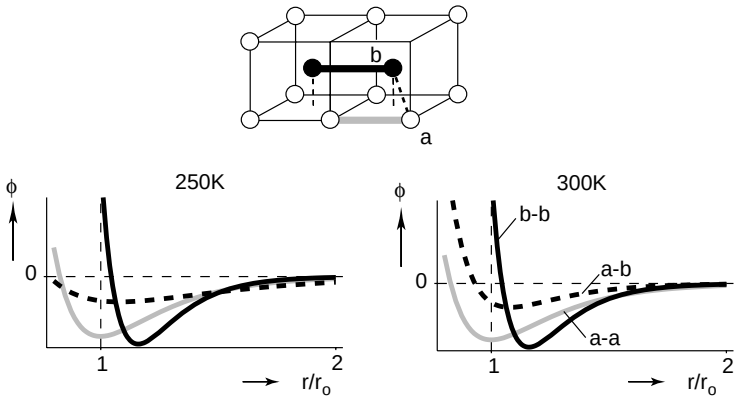

Fig. 6. Effect of temperature on the three pair-potentials.

deformation can be parameterized by the six lattice parameters, side lengths (a, b, and c) and internal angles (α, β, and γ). Temperature plays the role of a loading parameter. For each equilibrium path of interest the applicable degrees of freedom are first identified to characterize the branch uniquely, namely

$$\mathbf{U}_{\text{cubic}} = \begin{bmatrix} U_{11} & 0 & 0 \\ 0 & U_{11} & 0 \\ 0 & 0 & U_{11} \end{bmatrix}, \tag{4.1a}$$

$$\mathbf{U}_{\text{rhombo}} = \begin{bmatrix} U_{11} & U_{12} & U_{12} \\ U_{12} & U_{11} & U_{12} \\ U_{12} & U_{12} & U_{11} \end{bmatrix}, \tag{4.1b}$$

$$\mathbf{U}_{\text{ortho}} = \begin{bmatrix} U_{11} & U_{12} & 0 \\ U_{12} & U_{11} & 0 \\ 0 & 0 & U_{33} \end{bmatrix}, \tag{4.1c}$$

$$\mathbf{U}_{\text{mono}} = \begin{bmatrix} U_{11} & U_{12} & U_{13} \\ U_{12} & U_{11} & U_{13} \\ U_{13} & U_{13} & U_{33} \end{bmatrix}. \tag{4.1d}$$

The corresponding subset of the nonlinear equations (2.3) is then solved incrementally using Newton–Raphson iteration with path length control Δs.

$$\text{cubic} \qquad \Delta s^2 = (\Delta\theta/\theta^*)^2 + \Delta U_{11}^2, \tag{4.2a}$$

$$\text{rhombohedral} \qquad \Delta s^2 = (\Delta\theta/\theta^*)^2 + \Delta U_{11}^2 + \Delta U_{12}^2, \tag{4.2b}$$

$$\text{orthorhombic} \qquad \Delta s^2 = (\Delta\theta/\theta^*)^2 + \Delta U_{11}^2 + \Delta U_{12}^2 + \Delta U_{33}^2, \tag{4.2c}$$

$$\text{monoclinic} \qquad \Delta s^2 = (\Delta\theta/\theta^*)^2 + \Delta U_{11}^2 + \Delta U_{12}^2 + \Delta U_{33}^2 + \Delta U_{13}^2. \tag{4.2d}$$

To improve the numerical conditioning of the algorithm a scaling factor, θ^*, is introduced to ensure variations of the same order in temperature and deformation for a given Δs. This scheme allows limit loads to be easily traversed in the calculation.

The energy density of a representative volume element is summed explicitly according to Eq. (2.6) over all interacting bonds within a sphere of influence. The calculation is, therefore, long-range at the nano-scale. Practically, an Eulerian influence sphere of seven lattice units is sufficient to achieve converged results for our chosen pair-potentials.[8] The stability of equilibrium solutions can be evaluated by monitoring the number of negative eigenvalues of $\partial^2 W/\partial\mathbf{U}\partial\mathbf{U}$ through the use of a cyclic Jacobi method (see Patel, 1994).

4.2. Discussion of numerical results

Fig. 7 presents the calculated equilibrium paths as a plot of one internal lattice angle, γ (where $\cos\gamma = U_{1k}U_{k2}$), versus temperature, θ. The principal branch of the CsCl cubic crystal (red line) is shown with a constant value of $\gamma = 90^\circ$. At the reference temperature of 300 K the CsCl crystal is stable (indicated by the solid line), but becomes unstable (indicated by the dotted line) below 263 K. The critical point at 263 K is a triple bifurcation of Case III-type (see Section 3.3) that includes four intersecting rhombohedral paths and three intersecting orthorhombic paths. Only one of each are shown. Consistent with the previous asymptotic analysis the rhombohedral path (green line) is a transcritical (asymmetric) path that is initially unstable. The orthorhombic branch (yellow line) is a super-critical (symmetric) path that, in this case, is also initially unstable. As the temperature decreases below the critical point the rhombohedral path continues with an increasing γ that eventually levels off near $\gamma = 109^\circ$, but it remains unstable.

[8] One must beware of the temptation to attach the sphere of influence to a given set of atoms (Lagrangian sphere). Relatively large finite deformation may convect it into a distorted ellipsoid that introduces an artificial bias into the calculation. This can result in an aphysical imperfection that masks underlying bifurcations.

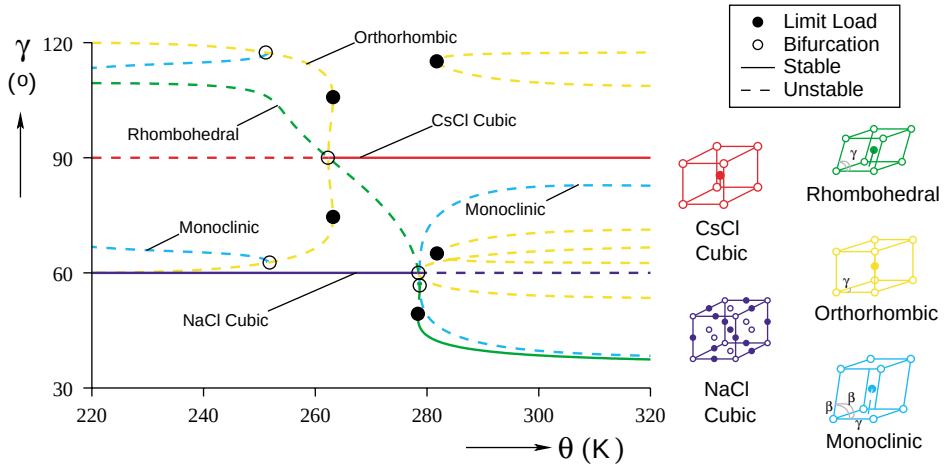

Fig. 7. Calculated equilibrium paths showing unit cell angle as a function of temperature.

As the temperature increases above the critical point the rhombohedral path continues with a decreasing γ that steepens as it crosses 60°. Each segment of the symmetric orthorhombic path emanating from the critical point on the CsCl branch undergoes a shallow limit load near $\theta=263$ K and then approaches $\gamma=60°$ and 120° for low temperatures. Both segments remain unstable, however, for the entire branch. Interestingly, a secondary (single) bifurcation point with an intersecting monoclinic branch (light blue line) occurs near $\theta = 251$ K, but it is also unstable.

As can be seen in Fig. 7 another equilibrium path exists at a constant $\gamma = 60°$ (blue line). This seemingly large distortion of the reference configuration actually represents another cubic crystal of the NaCl-type. Whereas the CsCl (or B2) crystal is two inter-penetrating simple cubic mono-atomic crystals, the NaCl (or B1) crystal is two inter-penetrating face centered cubic (FCC) mono-atomic crystals. The NaCl crystal is stable at low temperatures, but becomes unstable at temperatures above a critical temperature of $\theta = 278$ K. This critical point is also of the Case III-type with intersecting rhombohedral and orthorhombic branches. The rhombohedral path is a continuation of the path that intersects the CsCl primary branch, which eventually becomes stable for high temperatures. Notice also the isolated (detached) unstable orthorhombic paths that exist for temperatures above $\theta = 281$ K.

Since the behavior is relatively dense near the NaCl critical point, Fig. 8 shows an expanded view in this vicinity. The rhombohedral path is again a transcritical bifurcation and the orthorhombic path is a super-critical bifurcation of the NaCl cubic branch. The rhombohedral path undergoes two limit loads with decreasing γ, and becomes stable after the second limit load. The orthorhombic path is everywhere unstable. Notice also that the orthorhombic and rhombohedral paths are intersected by an unstable monoclinic path.

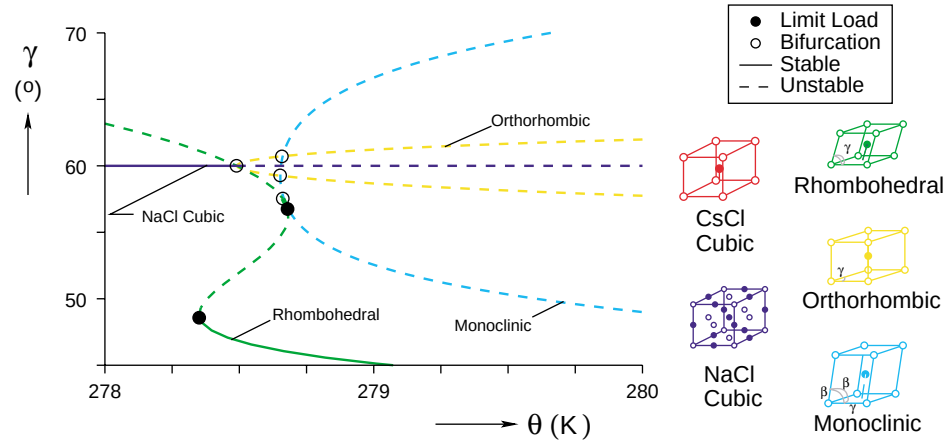

Fig. 8. Detail of equilibrium paths near NaCl multiple bifurcation.

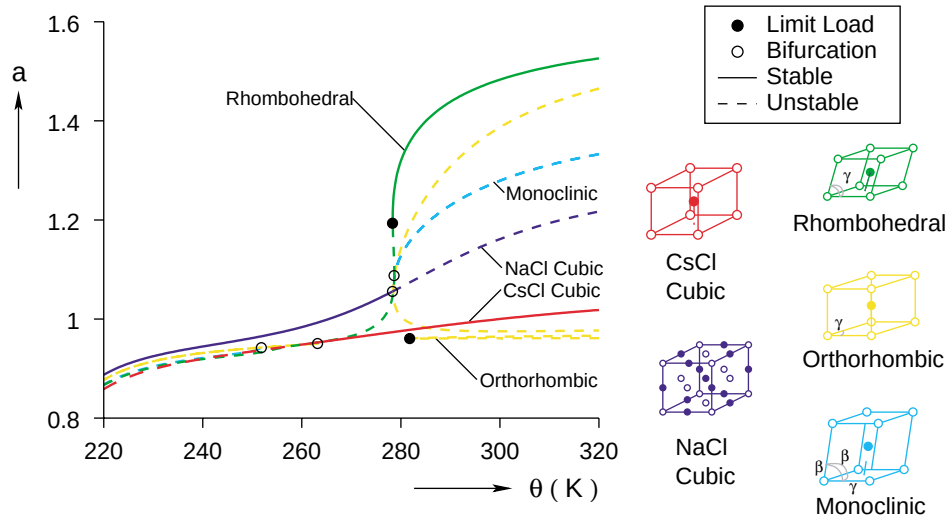

Fig. 9. Unit cell side-length.

Fig. 9 shows the dependence of the CsCl unit cell side-length, a (where $a = (U_{1i}U_{i1})^{1/2}$), with temperature for the equilibrium paths. It has been normalized to a value of unity at the reference temperature of 300 K. Although the side-length, $\sqrt{2}a$, for the NaCl crystal remains larger than that of the CsCl crystal for all temperature, the NaCl crystal actually has a more dense packing since it has twice as many atoms per unit cell. The stable rhombohedral segment has a dramatically increasing side-length with increasing temperature eventually leveling off near a value of $a = 1.53$.

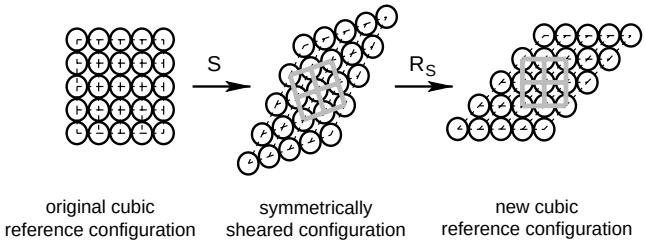

Fig. 10. Illustration of a reconstructive mode of a periodic lattice.

The existence of more than one cubic configuration separated by a rather large rhombohedral deformation is an interesting feature that merits discussion. This is a consequence of the periodic nature of the crystal and the fact that particular finite deformations exist which recover the cubic point symmetry of the crystal. As an illustration Fig. 10 depicts a 2-dimensional square lattice that is subjected to a particular symmetric shear deformation $\mathbf{S}$ that produces another square lattice (of infinite extent). The rigid body rotation $\mathbf{R}_s$ brings the new cubic axes (heavy gray axes) in line with the original ones (dotted axes). More possibilities exist in three dimensions. The deformation gradient $\mathbf{F}$ to the current configuration relative to the original reference configuration (dotted axes) can be related to the deformation gradient $\mathbf{F}^*$ to the current configuration from the new reference configuration (heavy gray axes) by

$$\mathbf{F} = \mathbf{F}^* \cdot \mathbf{R}_s \cdot \mathbf{S}. \tag{4.3}$$

Since the original reference configuration satisfies the symmetry condition ($\mathbf{M}$ is in the octahedral point group)

$$W(\mathbf{F}) = W(\mathbf{F} \cdot \mathbf{M}), \tag{4.4}$$

we seek particular deformations $\mathbf{S}$ such that the same symmetry is satisfied relative to the new reference configuration

$$W^*(\mathbf{F}^*) = W^*(\mathbf{F}^* \cdot \mathbf{M}), \tag{4.5}$$

where the energy of the crystal relative to the new reference configuration is defined as

$$W^*(\mathbf{F}^*) \equiv W(\mathbf{F}^* \cdot \mathbf{R}_s \cdot \mathbf{S}). \tag{4.6}$$

We call $\mathbf{S}$ the cubic reconstructive mode, since it is a rearrangement of rigid spheres into an equivalent point symmetry group. This is a special case of a *group–nonsubgroup*, or *reconstructive transformation* (see Tolédano and Dmitriev, 1996; Hatch et al., 2001), in which the two kinematically disjoint crystals (both cubic, in this case) are indirectly related by a common symmetry subgroup (rhombohedral). The cubic reconstructive

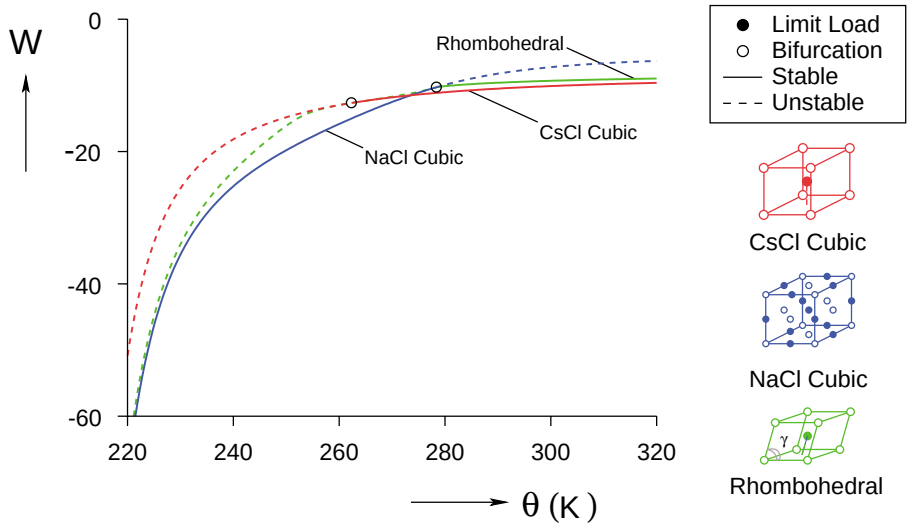

Fig. 11. Relative energy density of stable equilibrium paths.

mode that takes the CsCl cubic crystal to the NaCl crystal has

$$\mathbf{S} = \frac{1}{4}\begin{bmatrix} 4 & 1 & 1 \\ 1 & 4 & 1 \\ 1 & 1 & 4 \end{bmatrix}, \quad \mathbf{R}_s = \frac{1}{3}\begin{bmatrix} -1 & 2 & 2 \\ 2 & -1 & 2 \\ 2 & 2 & -1 \end{bmatrix}. \tag{4.7}$$

Similar CsCl–NaCl transitions to that suggested by Fig. 7 have been observed in several compounds including CsCl (near 460°C), and other alkali halides (see Buerger, 1951; Tolédano and Dmitriev, 1996).

The stable rhombohedral crystal that occurs above $\theta = 278$ K approaches another cubic crystal asymptotically as the temperature becomes large. This asymptotic crystal is another application of the above cubic reconstructive mode from the NaCl crystal. The rhombohedral crystal, however, never reaches this cubic crystal because of the ordering of the two atom species (alternating close packed planes of '*a*' atoms and then '*b*' atoms). This unusual ordering of atoms seems improbable, so we expect that it will not occur in reality.

Finally, the energy densities of the three stable phases, CsCl, NaCl, and rhombohedral crystals, are examined as a function of temperature as shown in Fig. 11. The lowest energy level is an indication of absolute stability at a given temperature. At high temperature the CsCl crystal has the lowest energy density, but at low temperature the NaCl crystal has the lowest energy density. The rhombohedral crystal is stable at high temperatures, but its energy level remains above that of the stable CsCl crystal. Consequently, the rhombohedral crystal is at best metastable.

From Fig. 11 one can imagine temperature-induced phase transitions between the CsCl and NaCl crystals. Starting at a high temperature (say our reference temperature of 300 K) the CsCl crystal is stable and has the lowest energy level. As the tem-

perature is decreased the energy level crosses that of the NaCl crystal at $\theta = 273$ K. Between this temperature and $\theta = 263$ K the CsCl crystal is metastable. At $\theta = 263$ K it looses stability and a transition to NaCl would occur as the temperature is decreased further. During this transition there is a jump in the energy level downward. Now consider starting at a low temperature in the NaCl phase and increase the temperature. The NaCl phase is absolutely stable until $\theta = 273$ K where its energy level crosses that of the CsCl branch. The NaCl phase is then metastable until it looses stability at $\theta = 278$ K, where a transition to CsCl occurs as the temperature is raised further. During such a temperature cycle, dynamic jumps in energy level occur wherever a phase looses stability. The overlap of stable phases leads to hysteresis in the transitions which is suggestive of typical martensitic phase transitions (See the austenite and martensite peaks, ignoring the R-phase peak, in Fig. 1). However, it should be emphasized that this CsCl–NaCl transformation is a reconstructive transformation due to the large deformations separating the phases and the group–nonsubgroup relationship between the symmetry groups of the two phases.

The results of the asymptotic analysis presented in Section 3 determine the tangents and curvatures of paths emerging from a bifurcation point and thus provide a nontrivial verification of the numerical calculations. Eliminating ξ from the expansions (3.16) results in θ as a function of U_{12}

$$\theta(U_{12}) = \theta_c + \left.\frac{\partial\theta}{\partial U_{12}}\right|_c U_{12} + \frac{1}{2}\left.\frac{\partial^2\theta}{\partial(U_{12})^2}\right|_c (U_{12})^2 + O((U_{12})^3). \tag{4.8}$$

For the rhombohedral and orthorhombic paths emerging from the CsCl cubic path in Fig. 7 we find

$$\left.\frac{\partial\theta}{\partial U_{12}}\right|_c^{\mathscr{R}\mathscr{H}_1} = -\mathscr{E}/\mathscr{E}_\theta, \tag{4.9a}$$

$$\left.\frac{\partial\theta}{\partial U_{12}}\right|_c^{\mathscr{O}\mathscr{R}_3} = 0, \quad \left.\frac{\partial^2\theta}{\partial(U_{12})^2}\right|_c^{\mathscr{O}\mathscr{R}_3} = -\frac{\hat{\mathscr{E}}}{3\mathscr{E}_\theta}. \tag{4.9b}$$

The values $\mathscr{E}$, $\mathscr{E}_\theta$, and $\hat{\mathscr{E}}$ are calculated (based on Eqs. (3.29) and (3.36)). The expansion (4.8) is plotted against the numerically determined equilibrium path for both the rhombohedral ($\mathscr{R}\mathscr{H}_1$) and orthorhombic ($\mathscr{O}\mathscr{R}_3$) phases (see Fig. 12). The expansions (3.16) agree well with the numerical results for the range $|U_{12}| < 0.05$.

A parameter study was also conducted to determine the sensitivity of the model. It was found that changes of up to 40% of any one of the parameters had only a quantitative effect on the results, i.e., the qualitative character of the results remained essentially unchanged. The most influential parameter was α_θ, which determines θ_c.

The results obtained so far are encouraging in that they seem to confirm that martensitic transformations are the results of instability phenomena at the nano-scale. In our case, however, the transitions occur between two cubic crystals, which is not the case

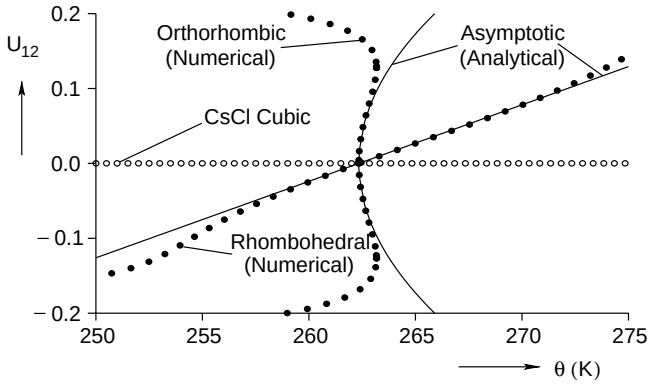

Fig. 12. Validity of asymptotic expansions (3.16).

in shape memory alloys. The lower symmetry crystals, such as orthorhombic and monoclinic, do appear in our calculations, but they remain unstable in our chosen temperature window. More work remains to be done. We suspect that the uniform deformation assumption is rather restrictive, and that relaxing internal degrees of freedom is necessary to capture the lower symmetry stable crystals that are actually observed in shape memory alloys. Relaxing the uniform deformation assumption would also admit the possibility of twinning phenomena and would be interesting to study in this context. The use of more sophisticated atomic potentials than simple pair-potentials would likely improve the realism of the calculations. Martensitic transformations are strongly affected by the application of an external stress, which we have so far ignored. Nevertheless, now that the framework exists, these missing ingredients can be added to improve the modeling of martensitic transformations at the atomic scale.

5. Summary and conclusions

An explicit energy density $W(\mathbf{F};\theta)$ is constructed for a bi-atomic crystal using pseudo-static, temperature-dependent atomic pair-potentials to investigate martensitic transformations as instability phenomena at the nano-scale. Equilibrium paths are calculated numerically for a uniformly deforming bi-atomic crystal of infinite extent under zero applied stress. Primary branches of crystals with cubic symmetry are identified, as well as intersecting branches of crystals with rhombohedral, orthorhombic, and monoclinic symmetries. Bifurcation points with multiple modes appear and asymptotic techniques are used to uncover the character and initial stability of bifurcated branches. The asymptotic analysis helps to guide the numerical results and gives results that, in some cases (initially unstable tetragonal and rhombohedral bifurcated paths), are independent of the potential model used, only depending on the symmetry of the crystal on the primary branch. This analysis determines which crystal structures emerge from

any particular critical point and characterizes the initial stability of these paths. These results cannot be obtained by symmetry considerations alone.

In the numerical results the stability of each branch is evaluated, showing that portions of three branches are stable: two cubic phases (CsCl and NaCl crystal structures) and one rhombohedral phase. The rhombohedral phase may not be realistic due to its improbable ordering for the two atomic species, and the stable portion of the equilibrium path is at best metastable relative to the stable CsCl path. The CsCl crystal (also the crystal structure of NiTi austenite) is stable at high temperature, while the NaCl crystal is stable at low temperature. The two stable CsCl and NaCl segments overlap for intermediate temperatures, suggesting the existence of a temperature-induced, hysteretic reconstructive martensitic transformation. Each cubic branch has a triple critical point with intersecting rhombohedral and orthorhombic paths. Using finite deformation kinematics the two cubic paths are shown to be connected by an unstable rhombohedral path.

While the current results are interesting and seem promising, it must be noted that the current model does not predict any temperature-induced proper martensitic transformations. The equilibrium paths with low symmetry, such as orthorhombic and monoclinic (which are observed in SMA martensites), are found to be unstable for all temperatures within our temperature window. Further improvements are necessary before a realistic model can be developed for martensitic transformations in SMAs at the atomic scale. Specifically, the kinematic assumption of uniform deformation should be relaxed to allow internal atomic shuffles, as is known to occur in SMA crystals; more sophisticated atomic potentials, such as multi-body potentials or the modified embedded atom method, could be used; and the effect of applied stress should be investigated, since martensitic transformations in SMAs are known to be sensitive to both temperature and stress. The framework now exists for these improvements to be made.

Acknowledgements

The financial support from a Computational Science Graduate Fellowship from the Department of Energy (for R. Elliott), a CAREER grant from the National Science Foundation (for J. Shaw), and a 1998 fellowship from the École Polytechnique (for N. Triantafyllidis) are acknowledged with thanks.

Appendix A. Determination of $\mathscr{E}_{IJKL}$

Determination of the coefficients in Eq. (3.36) requires the use of the fourth order terms (not shown) in the expansion (3.6) and the values $\overset{(IJ)}{\mathbf{V}}$ defined by Eqs. (3.19a) and (3.19b). The derivation of Eqs. (3.36) and (3.37) is detailed as follows.

From the definition of $\overset{(IJ)}{\mathbf{V}}$ in Eq. (3.19), using the results of Eq. (3.6) and notation introduced in Eq. (3.7), and making use of the eigenmodes in Eq. (3.14) one obtains a

relatively straightforward system to determine $\overset{(IJ)}{\mathbf{V}}$. More specifically, $\overset{(IJ)}{\mathbf{V}} = \mathbf{0}$ for $I \neq J$ due to the equilibrium condition (3.19a). With this information and the orthogonality condition (3.19b), Eq. (3.19a) may be reformulated (where no summations are implied) as

$$\begin{bmatrix} \overset{2}{L}{}^{c}_{nn} & \overset{2}{L}{}^{c}_{nn'} & \overset{2}{L}{}^{c}_{nn'} \\ \overset{2}{L}{}^{c}_{nn'} & \overset{2}{L}{}^{c}_{nn} & \overset{2}{L}{}^{c}_{nn'} \\ \overset{2}{L}{}^{c}_{nn'} & \overset{2}{L}{}^{c}_{nn'} & \overset{2}{L}{}^{c}_{nn} \end{bmatrix} \begin{bmatrix} \overset{(II)}{V}_{ii} \\ \overset{(II)}{V}_{jj} \\ \overset{(II)}{V}_{kk} \end{bmatrix} = -4 \begin{bmatrix} \overset{3}{L}{}^{c}_{n'ss} \\ \overset{3}{L}{}^{c}_{nss} \\ \overset{3}{L}{}^{c}_{nss} \end{bmatrix}, \quad II = ii \neq jj \neq kk \neq ii. \tag{A.1}$$

Solving this system of equations one obtains,

$$\overset{(II)}{V}_{ii} \equiv \eta = -4 \frac{\overset{2}{L}{}^{c}_{nn} \overset{3}{L}{}^{c}_{n'ss} + \overset{2}{L}{}^{c}_{nn'} (\overset{3}{L}{}^{c}_{n'ss} - 2\overset{3}{L}{}^{c}_{nss})}{(\overset{2}{L}{}^{c}_{nn} - \overset{2}{L}{}^{c}_{nn'})(\overset{2}{L}{}^{c}_{nn} + 2\overset{2}{L}{}^{c}_{nn'})}, \tag{A.2a}$$

$$\overset{(II)}{V}_{jj} = \overset{(II)}{V}_{kk} \equiv \hat{\eta} = -4 \frac{\overset{2}{L}{}^{c}_{nn} \overset{3}{L}{}^{c}_{nss} - \overset{2}{L}{}^{c}_{nn'} \overset{3}{L}{}^{c}_{n'ss}}{(\overset{2}{L}{}^{c}_{nn} - \overset{2}{L}{}^{c}_{nn'})(\overset{2}{L}{}^{c}_{nn} + 2\overset{2}{L}{}^{c}_{nn'})}. \tag{A.2b}$$

Finally, the results of Eqs. (A.2) may be substituted into Eq. (3.21b) and a lengthy calculation involving the fourth order term in the expansion (3.6) results in Eq. (3.36).

References

Abeyaratne, R., Chu, C., James, R.D., 1996. Kinetics of materials with wiggly energies: theory and application to the evolution of twinning microstructures in a Cu–Al–Ni shape memory alloy. Philos. Mag. A—Phys. Condens. Matter defects Mech. Properties 73 (2), 457–497.

Bhattacharya, K., 1998. Theory of martensitic microstructure and the shape-memory effect. Available from author: bhatta@co.caltech.edu.

Born, M., 1940. On the stability of crystal lattices. I. Math. Proc. Cambridge Philos. Soc. 36, 160–172.

Buerger, M.J., 1951. Crystallographic aspects of phase transformations. In: Smoluchowski, R. (Ed.), Phase Transformations in Solids. Wiley, New York, pp. 183–211.

Cohen, M., Olson, G.B., Clapp, P.C., 1979. On the classification of displacive phase transformations. Proceedings of International Conference on Martensitic Transformations, ICOMAT-79, p. 1.

Ericksen, J.L., 1992. Bifurcation and martensitic transformations in bravais lattices. J. Elasticity 28, 55–78.

Ericksen, J.L., 1996. On the possibility of having different bravais lattices connected thermodynamically. Math. Mech. Solids 1 (1), 5–24.

Hatch, D.M., Lookman, T., Saxena, A., Stokes, H.T., 2001. Systematics of group–nonsubgroup transitions: square to triangle transition. Phys. Rev. B—Condens. Matter 64:060104(R), 1–4.

James, R.D., 1986. Displacive phase transformations in solids. J. Mech. Phys. Solids 34 (4), 359–394.

Milstein, F., 1970. Mechanical stability of crystal lattices with two-body interactions. Phys. Rev. B—Condens. Matter 2 (2), 512–517.

Milstein, F., Hill, R., 1977. Theoretical properties of cubic crystals at arbitrary pressure—I. Density and bulk modulus. J. Mech. Phys. Solids 25, 457–477.

Milstein, F., Hill, R., 1978. Theoretical properties of cubic crystals at arbitrary pressure—II. Shear moduli. J. Mech. Phys. Solids 26 (4), 213–239.

Milstein, F., Hill, R., 1979. Theoretical properties of cubic crystals at arbitrary pressure—III. Stability. J. Mech. Phys. Solids 27 (3), 255–279.

Otsuka, K., Sawamura, T., Shimizu, K., 1971. Crystal structure and internal defects of equiatomic tini martensite. Phys. Status Solidi A—Appl. Res. 5 (2), 457–470.

Patel, V.A., 1994. Numerical Analysis. Saunders College Publishing, Fort Worth, TX, pp. 440–445 (Chapter 13).

Shaw, J.A., 2000. Simulations of localized thermo-mechanical behavior in a NiTi shape memory alloy. Int. J. Plast. 16 (5), 541–562.

Shaw, J.A., Kyriakides, S., 1998. Initiation and propagation of localized deformation in elasto-plastic strips under uniaxial tension. Int. J. Plast. 13 (10), 837–871.

Tolédano, P., Dmitriev, V., 1996. Reconstructive Phase Transitions. World Scientific, Singapore.

Triantafyllidis, N., Peek, R., 1992. On stability and the worst imperfection shape in solids with nearly simultaneous eigenmodes. Int. J. Solids Struct. 29 (18), 2281–2299.